Final Technical Report
US Geological Survey National Earthquake Hazards Reduction
External Research Program

USGS Award Number G11AP20029 (ASU) & G11AP20020 (SDSU)

Repeatability, accuracy, and precision of surface slip measurements from high-resolution topographic data: Collaborative Research with Arizona State University and San Diego State University

Prof. J Ramon Arrowsmith
School of Earth and Space Exploration,
Arizona State Univ.
Tempe, AZ, 85287-1404
E-mail: ramon.arrowsmith@asu.edu
Phone: +1 (480) 965-5081

Thomas K. Rockwell
Department of Geology
San Diego State University
San Diego, CA 92182
E-mail: trockwell@mail.sdsu.edu
Phone +1 (619) 594-4441

With significant input from J. Barrett Salisbury, David Haddad, Christopher Madden Madugo, Katherine Scharer, and Olaf Zielke

January 1, 2011 – December 31, 2011

No publications to report yet.

Abstract

Studies of active fault zones have burgeoned with the availability of high-resolution topographic data, particularly where airborne light detection and ranging (LiDAR) datasets provide a means to remotely analyze sub-meter fault geomorphology. Geomorphic features (e.g., stream channels) that cross a fault before a major earthquake can be measured after the event to determine earthquake slip at a point. Analysis of these and other offset features can provide useful information regarding earthquake slip at a point and can be used for generating earthquake slip distributions. Because these slip distributions are used for earthquake magnitude and hazard calculations, knowledge of the accuracy and precision of these measurements is of utmost importance.

We used a database of slip measurements that was recently compiled from many studies of active strike-slip faults (in California Uniform California Earthquake Rupture Forecast 3--UCERF3) to summarize existing field and LiDAR measurements of offset geomorphic features. We use the same database to compare existing field-based measurements with new LiDAR-

derived slip measurements where both exist for a particular landform, and we investigate the influence of natural variation and operator decisions on offset measurements using new LiDAR-derived measurements.

It is typically assumed that geomorphic features such as stream channels form more frequently than the surface-rupturing earthquakes that offset them; clusters of similarly displaced features are attributed to the number of earthquakes that have occurred since channel formation. We present new single-investigator field- and LiDAR-based measurements of fault-offset stream channels for the creeping section of the San Andreas fault (SAF) where large ground-rupturing earthquakes are not expected and therefore we have no expectation for consistent offsets. In an area with steady aseismic creep, one would expect a completely random distribution of offset channel magnitudes if channel formation is rapid, local, and random. We found 41 offset stream channels with a minimum offset magnitude of ~5 m, however, several 2-3 m offsets are present. This noticeable minimum-offset cluster of 5 m (similar to what we observe along the seismogenic portion of the San Andreas fault) suggests that for the entire creeping SAF, channel formation is systematic -- a result of widespread, climate-driven channel incision events. Furthermore, a steady creep rate of 35 mm/yr since 1862 (the "Great California Flood") results in almost exactly 5 m of displacement.

Finally, we present results of a LiDAR-based offset measurement study devised to test the repeatability of offset measurements made with different tools (e.g., paper image and scale, the Google Earth ruler tool, and a MATLAB GUI for calculating backslip required to properly restore tectonic deformation) by users of varying skill levels. Offset features are from various geographic regions and span a range of quality and complexity. We received 11 paper-, 28 Google Earth-, and 16 MATLAB-based survey responses, though not all individuals measured every feature provided. For all survey methods, the majority of responses are in close agreement. However, large discrepancies arise where users interpret landforms differently -- specifically the pre-earthquake morphology, total offset accumulation, and degradational evolution of offset geomorphic features. Experienced users make more consistent measurements, whereas beginners less-consistently choose the same interpretation for an offset feature. The Google Earth survey, for example, shows that the average percent difference between all expert measurements is significantly smaller (19%) than the percent difference between all beginner measurements (39%). Standardizing measurement and reporting methods is a crucial first step towards enhancing consistency of LiDAR-based analyses of active faults and establishing community protocols for measurement and reporting.

Introduction

Active faults are geomorphically expressed in different ways (e.g., Wallace, 1968, 1990; Burbank and Anderson, 2001; McCalpin, 2009). Where a predominant sense of slip persists, horizontally and vertically displaced geomorphic features can be used to constrain cumulative slip after the formation of the landform (Figure 1). If the long-term slip history and landform development processes are understood, the surface slip distribution from recent earthquakes can be reconstructed. Such information is essential for estimation of paleo-earthquake magnitudes and the formation and evaluation of conceptual models for earthquake recurrence and along-fault slip accumulation (e.g., Shimazaki and Nakata, 1980; Sieh and Jahns, 1984; Schwartz and Coppersmith, 1984). Assuming a direct relation between coseismic surface and sub-surface slip, along-fault surface slip distribution and slip accumulation patterns may serve as a proxy to constrain properties of the underlying fault plane (Scholz, 2002). The high-resolution topography provided by light detection and ranging (LiDAR) datasets that cover the topography along major active faults of western North America represent the corresponding fault-related geomorphology in unprecedented detail. While the ultimate reconstruction of slip in an earthquake using these data will come from comparisons of data from before and after the next great earthquake (e.g. Oskin, et al., 2012 and Nissen, et al. 2012), the reconstruction of offset landforms depicted in them provides a new and objective approach to also constrain past earthquake surface slip and slip accumulation patterns.

For this study, we focus primarily on major strike-slip faults where geomorphic features that developed roughly normal to the fault strike are horizontally displaced by repeated surface-rupturing earthquakes. Most of the offset features we discuss are of fluvial origin (e.g., channel walls, thalwegs, alluvial fans, landslides, terrace treads and risers) and are comprised of elements that can be projected to the fault plane and used as piercing lines to estimate fault slip. Given that surface-rupturing earthquakes along strike-slip faults typically produce offsets of 1-10 m (Wells and Coppersmith, 1994), ephemeral channels of 10^0-10^2 m width are typically the focus of reconstructions of recent slip histories (e.g., SAF: Wallace, 1968; Sieh, 1978; Lienkaemper, 2001; Zielke, et al., 2010, 2012; Garlock Fault (GF): McGill and Sieh, 1991; San Jacinto Fault (SJF): Salisbury, et al., 2012; Elsinore Fault (EF): Rockwell and Pinault, 1986; Rockwell, 1990; Talas Fergana fault: Trifonov, et al., 1992; Altyn Tagh Fault (ATF): Washburn, et al., 2001; Fuyun Fault: Awata, et al., 2010; Klinger, et al, 2011; North Anatolian Fault (NAF): Kondo, et al., 2005, 2010; Bocono Fault: Audemard, 2008; Denali 2002 earthquake: Haeussler, et al., 2004; see also reviews by McCalpin, 2009; Yeats, et al., 1997; Burbank and Anderson, 2001).

However, the fidelity of these landforms to record offset depends not only on their geometries but also on their post-offset erosional and depositional modifications (e.g., Cowgill, 2007). Immediately following tectonic perturbations, offset channels respond with altered patterns of channel degradation and aggradation. In some instances, streams with high transport capacity may bury or erode tectonic displacements completely. The size of the channel, therefore, as a proxy for its power, will control the magnitude of displacements that can leave their mark (e.g., Wallace, 1968, Ouchi, 2004).

Inherent to reconstruction of recent fault offset using landforms are two major assumptions: 1) the slip along faults occurs co-seismically (with no significant contribution by fault creep), and 2) landforms develop at the decadal timescale while earthquakes occur at the centennial timescale so that groups of relatively similar offset magnitudes correspond to successive ground-rupturing events. The latter assumption has been recently challenged by results that suggest that feature formation rates in some environments may be less frequent than previously assumed (Grant-Ludwig, et al., 2010). In these scenarios, slip per event over time may vary significantly at a location, thus only the largest earthquakes dominate the discrete offsets while smaller events still break the surface and contribute to the number of events in paleoseismic investigations (e.g., Zielke, et al., 2010; and Akciz, et al., 2010).

Several recent studies have highlighted the scientific potential of high-resolution topographic data sets in the reconstruction of coseismic surface slip histories and in the formulation and evaluation of earthquake recurrence and forecasting models (e.g., ; WGCEP, 2008; Grant-Ludwig, et al., 2010; Zielke, et al. 2010, 2012; Salisbury, et al., 2012). LiDAR data for the major faults of the SAF system as well as sections of other active faults around the world are widely available in addition to several useful computational tools, including those developed by Zielke and Arrowsmith (2012). High resolution satellite and aerial photographic imagery is also used for offset reconstructions (e.g., Klinger, et al., 2011 and Rockwell and Klinger, in press). While there is an increasing availability of data and resources for surface slip reconstructions, the resulting models of fault behavior are only as good and reliable as the individual measurements upon which they are based. We therefore have examined the influence of natural variation and operator decisions on offset measurements in order to improve surface slip histories for investigated faults, and to provide a better understanding of fault behavior and along-fault slip accumulation.

Methods

Offset channel measurements

An offset measurement typically contains multiple parts: the quantitative measurement of the offset feature, the quantitative uncertainty of that measurement, and a qualitative assessment of the confidence associated with the determination. The assessment of the tectonically displaced feature requires delineation of several geomorphic components including the fault trace, the offset landform elements (e.g., the channel margins and thalweg), as well as the projection lines of those individual landform elements into the fault plane. Offset measurement is determined by along-fault differences in landform element projections. Quantitative uncertainty in the offset comes from assessment of the minimum and maximum credible offset reconstructions. The uncertainty in that reconstruction is primarily dependent on the size and preservation of the geomorphic feature and associated offset. For a complete description of the analytical tools and methods used to generate new measurements, please see: "Measuring Earthquake-Generated Surface Offsets from High-Resolution Digital Topography" in our online appendix http://stockdale.sese.asu.edu/slip_project/Measuring_surface_offsets_from_LiDAR.pdf and Zielke and Arrowsmith, 2012.

The confidence or quality rating is a subjective assessment made by the geologist and depends not only on the size and preservation of the geomorphic feature and associated offset, but also on the simplicity of landform projections and fault trace delineations. This quality assessment has been used to weight offset measurement probability distribution functions, emphasizing highly reliable measurements (e.g., McGill and Sieh, 1991; McCalpin, 2009; Zielke, et al., 2010; Madden, et al., 2012).

Analysis of compiled offset measurements for the Uniform California Earthquake Rupture Forecast 3

The Working Group on California Earthquake Probabilities has undertaken the Uniform California Earthquake Rupture Forecast 3 (UCERF3; www.wgcep.org). As a part of this substantial effort, many databases describing the active faults and earthquake potential of California were developed or updated. Of great value to our validation effort is the Compilation of *Slip in the Last Event Data and Analysis of Last Event, Repeated Slip, and Average Displacement for Recent and Prehistoric Ruptures* (Madden, et al., 2012). This UCERF3 slip-per-event database focuses on California's fastest slipping strike- and dip-slip faults, combining existing historic, prehistoric, paleoseismic, and geomorphic data for single and multi-event offsets

with new remote measurements. The existing measurements are from published fault studies, gray literature, and publications in preparation. For other high-priority faults, new measurements are from analyses of LiDAR datasets for micro-geomorphic (meter-scale) offsets in active fault zones. For the purposes of data compilation from numerous sources, each database entry was assigned a quality rating from 1 to 3, where 1 is high (best) quality, and 3 is low (worst) quality. Quality ratings of existing measurements were translated to this more simplistic, standardized rating scale by Madden, et al. (2012). Together, these new and existing measurements provide a significant contribution to the Uniform California Earthquake Rupture Forecast database – the basis for the UCERF3 hazard model. The Madden, et al. (2012) report presents the database and analyzes its implications with respect to recent fault slip in California as well as firmly establishes reporting and interpretation methods for offset data. In this study, we use the rich UCERF3 slip-per-event database as a part of our examination of repeatability, precision, and accuracy of surface offset data.

We approach the evaluation of field and remotely determined offsets in a number of ways. First, we utilize the recently compiled UCERF3 slip-per-event database to summarize traits of existing field and LiDAR measurements of offset geomorphic features (Madden, et al., 2012). For this purpose, we recognize the number of component measurements (i.e., individual horizontal and vertical slip measurements) in addition to the number of unique geographic measurement sites. In many instances, multiple measurements were made at the same location (e.g., horizontal and vertical displacements recorded by the channel thalweg and one or two of the channel margins). In many instances, multiple measures using different methods (LiDAR, field, etc.) exist for the same offset geomorphic feature, providing an excellent opportunity to compare the consistency and reliability of earthquake slip measurements at a point. This unprecedented data set represents the best accumulation of data from a variety of investigators, faults, environments, base maps, and quality rating schemes available.

We use the same database to compare existing field-based measurements with LiDAR-derived slip measurements where both exist for particular landforms, and we analyze new LiDAR-derived measurements made specifically for the UCERF3 effort. In this report, a measurement generated for the UCERF3 database (or in a similar style – a measurement with associated uncertainty and semi-quantitative quality rating) will be referred to as a "new measurement (NM)."

Offset measurement validation experiment

The use of high-resolution LiDAR data for remote fault analysis has recently been developed and implemented in studies of the central SJF and the 1857 rupture extent of the SAF (Salisbury et al., 2012, Zielke et al., 2012) but there is a lack of consistency between users both for data analysis and results reporting. There is an increasing need to standardize and to uniformly validate measurements. How reliable and repeatable are offset measurements? What controls the variation in measurements and how much depends on the observer? Offset measurements of tectonically displaced geomorphic features are typically made by individual investigators, yet there is no coherent understanding of the effects of terrain type, geomorphology, vegetation, data type, etc. on the reliability and repeatability of the measurements from observer to observer.

In the second major portion of this project, we explored the repeatability of offset measurements under controlled conditions by inviting the participation of colleagues, interested geoscience community members, and the general public to measure up to ten geomorphic offsets (using high resolution topography as a base). We chose different offset features from major active faults in western North America; features vary in age from 2 to hundreds of years old and are of excellent to poor quality. All offsets were along northwest trending right-lateral faults (Figure 2). We have Institutional Review Board approval from Arizona State University for these human subjects surveys. Survey responses (including mapped fault traces and piercing lines) were anonymously submitted to an online database along with user experience information.

Along with the measurement results from the surveys, we collected information about the experience levels of the participants with three questions. The first question asked about general experience level:

1) I have no prior experience whatsoever.
2) I am familiar with the basic geologic principles and/or high-resolution topographic data.
3) I have measured offset geomorphic features in the field or with high-resolution topography/imagery.
4) I have extensive experience measuring offset features in the field or with high-resolution topography/imagery.

The second question gathered information about the data types that the person may have previously used to measure offset features (in the field, aerial photography, satellite photography, topographic maps, and high-resolution digital elevation models) and how the measurements were made (tape measure/ruler, total station, Google Earth, ArcGIS, LaDiCaoz—Zielke and Arrowsmith, 2012 Matlab-based tool, or other). The third question asked about classroom experience and if the person had taken or taught Field Geology, Geomorphology, Earthquake

Geology, Quaternary Geology, Tectonic Geomorphology, or Geographic Information Systems (GIS).

Two important controls on the quality rating of an offset are the obliquity between the offset feature elements and the fault zone and the fault zone width (indicator of complexity). We provided a semi-quantitative quality-rating rubric (Figure 2). The two-element quality was reported first based on relative obliquity and then on fault zone width (e.g. for a channel at 25 degrees to a well defined narrow fault trace: "low-high"). We did not have much compliance by the participants in reporting their quality ratings.

We devised three versions of the surveys: paper image and scale, the Google Earth ruler tool, and a MATLAB GUI for calculating backslip required to properly restore tectonic deformation. The different surveys used the same ten geomorphic features, but the difference in method reflects the range of work styles and experience levels of scientists doing this kind of research.

The paper-based survey is designed to be suitable for classroom dissemination but it could be used by an individual participant (Figure 3). The survey was filled out by hand and the document was mailed to us. The survey was used in classrooms at Potsdam University in Germany and at San Diego State University. Each image consists of a combination of three Light Detection and Ranging-derived (LiDAR-derived) products: an opaque "hillshade," a transparent digital elevation model (DEM), and a contour map. Map scales ranged from 1:175 to 1:800 and contour intervals from 10-100 cm. The participants were asked to trace the fault and geomorphic feature(s) (e.g., channel thalweg, channel margins, bar crest, etc.) used to estimate tectonic offset. The participants were told that the offset was along a northwest-trending right lateral fault, but there was no annotation of the figure to indicate the offset itself (Figure 3). Some images contain multiple offset features. Each page has a scale bar on the bottom right corner that was torn off and used for measuring. The participants were asked to report the offset and the measurement uncertainty magnitudes and to rate the overall quality of the offset feature (Figure 2).

The Google Earth-based measurement survey was popular because of the convenience of the software. It is possible to zoom to each site, view the topographic imagery and contextual image data, delineate features, and measure offsets. We saved the map images from the paper survey as *.kmz files and provided them for download from the survey site. The survey instructions included step-by-step text as well as short video tutorials on the use of Google Earth for this application. For each site/image, the participants

1) zoomed to the site,
2) defined the fault and offset features as paths for at least one offset (but they were

encouraged to do more),

3) measured the offset features using the ruler,
4) and saved the result from the ruler tool. The measurement was titled according to the feature measured (e.g., "channel thalweg measurement") and a quality rating and any other comments were included the measurement path description.

The resulting measurements were saved as a location in Google Earth (*.kmz file). The participants completed the experience survey and then anonymously uploaded the measurement *.kmz file to our database.

The "Lateral Displacement Calculator" (LaDiCaoz) is a MATLAB-based software tool with a graphical user interface developed for direct interaction with digital elevation models to measure and record horizontal offset (Zielke and Arrowsmith, 2012). The third (and most advanced) survey type was for participants who preferred to make their measurements using LaDiCaoz. We provided the raw digital elevation model files for each of the 10 sites, along with basic instructions but assumed that the participants knew LaDiCaoz already. To ensure that the participants measured the same offsets, we annotated the target on the topographic images in a circle as a guide. LaDiCaoz allows users to save their results, including the measurement, the amount of measured offset, and the quality rating. These results were uploaded to our server as the participants complete the experience survey.

While the available measurement methods spanned a range of complexity, most of the submitted responses were generated in Google Earth. We sifted the results manually and compiled the offsets, uncertainties, and ratings. Measurements are grouped according the geomorphic feature measured, as some sites contained multiple features. In the case of the Google Earth results, we also collected the paths that the participants used to delineate the fault zone, and offset landform elements and compared them graphically. Henceforth, a measurement generated by an anonymous user with our online survey will be referred to as an “online measurement (OM).” In a future portion of this study (planned for Fall, 2012), we will assess repeatability of field measurements (with high resolution topographic base maps) in a controlled field experiment with ~30 observers. See Scharer et al, *2012*, for a complete description of the field-based measurement validation activity.

Results

Overview

The UCERF3 database and our measurement experiment survey provide a rich suite of data to build our understanding of the repeatability, accuracy, and precision of offset measurements. We start our presentation of the results with our exploration of the UCERF3 database and its measures of offset magnitude, uncertainty, and quality, as measured from different physiographic settings by different investigators using LiDAR and field-based approaches. As part of the data accumulation for UCERF3, Salisbury measured offsets along the creeping section of the San Andreas fault, where large earthquakes are not expected. Some of the sites were also visited in the field. We discuss this subset of the database as a focused example from a single investigator measuring in an environment of no preexisting expectations, which might bias the search for offsets. Transitioning from the UCERF3 examination, the final set of results comes from our measurement experiment survey, which included both on-line and hard copy elements.

Analysis of the UCERF3 offset database

In total, there are 4,918 component measurements (i.e., individual horizontal and vertical slip measurements) made at 1,522 unique geographic locations along 37 UCERF3-defined fault strands (Figures 4a, 4b, and 5b, 5d; Madden, et al., 2012). The majority of measurements in the database are from field studies (i.e., historic earthquake surface rupture studies), but a substantial portion of measurements attributed to early historic (before 1900 A.D.) and paleoseismic earthquakes are from a combination of field and LiDAR studies (Figures 4 and 5). Most measurements in the UCERF3 database are of the highest quality rating (1), owing in large part to the fact that many existing offset measurements had no initial quality rating and the high quality ratings were assigned during the UCERF3 compilation (Madden, et al., 2012). Of the total component measurements, 2,759 are from historic earthquake ruptures and 2,159 are from prehistoric earthquake ruptures. The measurement methods differ significantly for these two groups. Historic earthquake slip measurements are dominated by field-based measurements, whereas the majority of prehistoric earthquake slip measurements are a combination of field- and LiDAR-based measurements, or one of the two (Figure 5a, 5c). More than half of the prehistoric earthquake fault data (16 of 25 strands) are from paleoseismic excavations with relatively few data points. Slip measurements in these cases are made from sub-surface channel or structural reconstructions with a wide range of uncertainties (Figure 5d). In most cases, the ratio of individual measurements to geographically unique measurement locations is roughly 1:1, but for some faults there are significantly more measurements than measurement sites (Figure 5b, 5d).

This is particularly apparent along the prehistoric SJF and GF ruptures, where there exist both field and LiDAR measurements for the same set of features. For historic ruptures such as the Emerson fault (1992 Landers earthquake), there are many sites with both horizontal and vertical measurements made for the same geomorphic feature.

We note a crude correlation between offset magnitude and associated uncertainty up to ~10 m of offset. (Figure 6). For the smallest field-based measurements (millimeter- and centimeter- scale historic earthquake ruptures) there are often no measurement uncertainties assigned. However, where more than ten offset measurements are presented with uncertainties, the slope and R^2 value describing the linear regression of the data are shown in Table 1. Where it can be determined, the field-based historic earthquake measurements tend to have lower uncertainties for a given offset than the prehistoric earthquake measurements, the majority of which are made remotely (Table 1). It should be noted that many investigators, using a variety of methods, made these offset measurements and uncertainty estimates in a wide range of geographic conditions.

On the other hand, the NM's generated for the UCERF3 database all used similar methods and reporting schemes, albeit they were made along different faults by different investigators. These measurements are for paleoseismic earthquakes. Where the quality and uncertainty reporting is standardized, we compare the relative individual quality ratings and compare the average uncertainty window (difference between the maximum and minimum acceptable offsets for a given geomorphic feature) associated with a group of displacement measurements with the same quality rating (Figure 7). In every scenario, the quality ratings are dominated by medium (2) ratings. In fact, for these newly acquired data, the highest quality ratings are the least common, and except for the case of the Elsinore Fault (EF), the low (3) quality measurements fall somewhere in between high (1) and medium (2) (Figure 7a). Figure 7b shows the average uncertainty window for each quality group of measurements. We average these windows for an entire group of similar quality measurements, and the standard deviations are shown (Figure 7b). The averages and standard deviations of the uncertainty windows are heavily influenced by the average magnitude of the displacements, which are shown by the red bars. The SAF and GL have relatively similar average uncertainty windows, but for the SAF where the offset magnitudes are all greater than 10 m, the standard deviations of the average windows are much greater. Additionally, there are significantly more measurements for the SAF. Interestingly, the SAF is the only fault system with increasing uncertainty window sizes as quality worsens.

We have a number of examples of field measurements that could be compared with LiDAR-based measurements of the same landforms. Zielke, et al. (2010) compared Sieh's (1978) mostly field-based measurements of offset along the SAF with Zielke, et al.'s (2010) using LiDAR. Salisbury, et al. (2012) presented a comparison of field and two different LiDAR-derived measurements for numerous targets (Figure 8). In this study, Haddad compared his measurements using LiDAR along the Garlock Fault with field measurements of McGill and Sieh (1991) (Figure 8). We also compared our field and the Salisbury LiDAR measurements from the creeping section of the SAF (see below). In general, these repeated observations are well correlated within error of the individual measurements (Figures 8 and 9). Salisbury, et al. (2012) showed that in some cases the field measurements were systematically lower than those from the LiDAR survey and attributed this to the synoptic perspective available from the remote view. Lienkaemper and Sturm (1989) and Lienkaemper (2001) suggested that over time, the geomorphic smoothing of the offset segment of a stream channel tends to cause the field observer to see lower magnitudes of offset.

A proxy for the geomorphic smoothing of the offsets at a point can be the mean annual precipitation (MAP). While climate has varied over the last millennium in California, the spatial variation in decadal MAP probably provides a useful relative gauge of the vigor of geomorphic smoothing in the UCERF3 database. Figure 9 shows a plot of the offset % uncertainty for a suite of offsets as a function of MAP along the corresponding fault reach. A modest increase in single-investigator uncertainty with increasing MAP indicates that geomorphic conditions associated with more arid sites produce and degrade landforms in a manner more likely to preserve offset features.

New measurements from the creeping section of the San Andreas Fault

We present the results of a NM study along the creeping portion of the SAF where large, ground-rupturing earthquakes are not expected to occur, nor have they for the past ~150 years. We argue that throughout this reach, there can be no anchoring or confirming biases (i.e., pre-existing expectations) for offset measurements given that it is unknown whether this reach can produce ground-rupturing earthquakes, and if so, if they repeat with similar slip (i.e., characteristic earthquakes). We measured offset channels throughout this reach from Parkfield to San Juan Bautista, CA in both the field and with LiDAR data (Figures 10 and 11). The LiDAR analysis was performed more than six months prior to fieldwork without ever visiting the area. The existing measurements were not taken to the field but the LiDAR-derived maps were used as

aids in the field. Due to landowner issues and time constraints, not every feature measured in the LiDAR data was visited in the field.

Contrary to the general conclusions from our examination of the UCERF3 database, our field uncertainties were relatively higher than those derived from LiDAR for repeated measurements (Figure 10a). The numerous offsets along the creeping section include a grouping at 2-5 m in the region about 120 km northwest of Parkfield.

The creeping section observations included measurements of fault zone width (Figure 11). The offset magnitude and the uncertainty window (difference between the maximum and minimum acceptable offsets for a given geomorphic feature) increase with increasing deformation zone width. We defined the Average Uncertainty Index (AUI) as an average of the ratios between the channel segment length, as locally evident approaching the up and downstream sides of the deformation zone, and deformation zone width for both the upstream and downstream channel segments (Figure 11). AUI decreases rapidly with deformation zone width and offset magnitude.

Analysis of the offset measurement validation experiment

Measurement survey responses (including mapped fault traces and piercing lines) were anonymously submitted to an online database, and user experience level information was recorded. We received responses from 55 individuals from all levels of proficiency as well as from a repeated application of the paper exercise in an undergraduate and graduate geomorphology course at the San Diego State University supervised by Rockwell. Of the 55 individuals who responded, 28 participants (from all levels of proficiency) used the Google Earth part of the validation experiment. Given the dominance of the Google Earth-based results, we emphasize them in the following discussion (Figure 12). Note that some of these features are from the creeping segment of the SAF and exhibit forms that are typically associated with surface-rupturing earthquakes (#s 2, 6, 9, 10). Even though we provided a simple quality rating scheme (Figure 3), few of the participants reported estimates of measurement quality or corresponding measurement uncertainties. In some cases, quality descriptions were qualitative rather than objective, based on the rubric. While a rubric of this sort is helpful, it is insufficient for adequate offset feature classification. In some cases, offsets received quality high ratings according to our rubric but associated user confidence was still low (if the tectonic nature of the offset was ambiguous, for instance).

Most reported measurements are in close agreement with one another (Figure 12a). The standard deviations and percent differences of averaged offset measurements have been grouped

and colored by skill level for each of the offset features (arranged according to offset magnitude). Except for a few instances, the standard deviations generally increase with increasing feature size and total displacement. We examined the relationship between self-reported experience level (no prior experience to extensive experience) in measuring offset geomorphic features with high-resolution topographic data) and uncertainty for each of the 10 measurement sites (Figure 12a). Inexperienced users have difficulty interpreting the pre-earthquake morphologies and total offset accumulation of a feature. These issues can be seen in responses to features 3 and 6nw (Figure 12). Feature number 8 shows the advanced group in stark disagreement with the less experienced participants.

The classroom portion of the validation experiment reported here was run at San Diego State University. The group of undergraduate and graduate students were in an upper-level geomorphology course (Figure 13). The experiment was applied twice to the same group of students: first prior to an introductory lecture on strike-slip faulting and the second a week later after receiving some instruction on how to recognize and measure offsets. In addition, a second set of undergraduate students used a Matlab-gui called "lateback" at the University of Potsdam in Germany, supervised by Zielke. The late-back gui is simpler than LaDiCaoz in that it allows the fault to be defined and the topographic image progressively backslipped. The observer can decide what magnitude of back slip gives the best reconstruction.

The results of the classroom repeated paper measurement experiment did not show a marked change in offset measurements (of the ten channels, five average displacement measurements increased and five decreased). Similarly, the standard deviations of the offset averages were split. Surprisingly, the average uncertainties for 8 of the 10 offset features significantly increased after the introductory lecture. Conversely, the standard deviations of the average uncertainties for 8 of the channels decreased. In general, the change in average quality estimates was more or less neutral. The standard deviations of the average quality estimates decreased, however, from run 1 to run 2. Lateback users consistently underestimated offset magnitude compared to the paper runs.

Discussion

Difficulties in Measurement-making

There are a number of observations we can make that relate to individual's ability to "get the right answer". First off, the orientation over which a feature is measured can result in a significant in the measurement value. Rockwell and Klinger (2013) show that for the 1940 Imperial fault rupture, making consistent measurements at different azimuths does not affect the

overall estimate of average displacement, but local displacements can vary by as much as a meter along sections of rupture that experienced 4 to 6 m of offset. In our validation experiment, we note that significant variation in displacement magnitude is evident from differences in the orientation of the feature relative to the fault trace. Although a range of measurements is typically acceptable (offset and symmetric/asymmetric offset uncertainty), the range of offsets can be reduced if all measurements are made either parallel to the local fault trace, or parallel to the regional fault trace.

Another significant variable is the distance over which features are projected into and across fault zones, and the width of the zone itself. Narrow (localized) faults require little or no projection and measurement is relatively straight-forward. In contrast, a broad zone of faulting may lead to large measurement uncertainty when the feature being measured is small or non-linear. A small rill or stream channel, for instance, may have some sinuosity that will bias the measurement. Similarly, is it best to use the center of such features (channel thalweg) or the two channel margins, or all three. It is our experience that the more features that are measured, the more consistent the result and the more accurate the portrayal of uncertainty.

Operator Biases

Our interest in the validation of geological measurements is not new. Bond, et al. (2007) conducted a similar study focusing on various interpretations of seismic data by users with various levels of expertise. In their attempt to quantify the subjectivity of seismic interpretation, they define the term "conceptual uncertainty" as the range of concepts that geoscientists could apply to a single dataset. Bond, et al. (2007) argue that this conceptual uncertainty must become a part of the resulting geologic models, being nearly as important as individually reported uncertainties themselves. Bond, et al. (2007) concluded that a range of factors influence how an individual's prior knowledge will affect interpretations, but that particular biases are as pervasive for those with 15+ years of experience just as they are for those with very little experience. In particular, two types of biases are nearly unavoidable: anchoring and confirmation biases. An anchoring bias is the failure to depart from initial ideas, whereas the confirmation bias involves actively seeking facts that support one's own beliefs or hypotheses, while actively disregarding conflicting observations. In fact, those with more experience are likely to *ask* for confirmation biases, or some sort of a starting point (e.g., "where in the world is this?"). Weldon, et al. (1996) (Chapter in McCalpin, p. 295) have similarly cautioned "… bias could be derived from the unconscious choice of a best match of uncertain features that is consistent with previous choices. This statement is not meant to suggest any impropriety in the data collection, but to acknowledge

that it is extremely difficult to avoid bias where measurements of 'matches' involves interpretation of the exact location of the feature being measured. From experience we know that after one finds several convincing offsets, one's eye is keyed to looking for matches in that range, so that one will often overlook or misinterpret offsets that are unexpected…" In the case of offset channels and our experiments, the novices had fewer biases as well as less of a trained eye to find and interpret features. On the other hand, experts can identify and interpret features easily but they also have more pre-existing expectations from the offset range to expect. The prevalence of these biases necessitates the establishment of a proper framework for making offset measurements, both in the field and remotely.

Others (Bond et al., 2007, 2010) have shown that professional experience does not necessarily guarantee a more correct interpretation. In these specific instances, however, the "correct" interpretation was known: synthetically generated structures in seismic data were used to test individuals' interpretations. For this study, we don't have the "correct" answer. Instead, we rely on the most commonly accepted interpretation as the "correct" answer. However, as in the case of Lienkaemper et al. (1989) and WGCEP (1988), is has been shown that professional opinions don't necessarily agree and contradictions regarding interpretation of the geologic structures/features exist. For example, feature number 8 in the Google Earth online survey shows the advanced group is in stark disagreement with the less experienced participants, and feature number 4 shows a disagreement among only those that deemed themselves "experts."

Natural lateral variability of offset magnitude in surface ruptures

There are now several studies that have demonstrated significant lateral variability in strike-slip offset along historical surface ruptures. Using long fence lines and orchards of planted trees, Rockwell et al. (2002) showed a 20-30% variability in offset along the 1999 Izmit rupture over short spatial distances of tens to hundreds of meters. Similar variations were observed along the 2010 El Mayor-Cucapa rupture in Mexico, using "Cosi corr" (optical correlation) technology (Leprince et al., 2011), with kilometer-scale and 15 km-scale systematic variabilities. In a reassessment of the 1940 Imperial fault rupture, Rockwell and Klinger (2013) used hundreds of closely spaced crop rows and orchard tree alignments to measure lateral displacement and also note about 30% lateral variability over spatial dimensions of tens to hundreds of meters. All of these observations are consistent with earlier mapping along historical surface ruptures, but in previous cases, it as commonly assumed that the variability was due to the inability to measure the full field of deformation. In contrast, the measurements using long crop rows that extended tens to hundreds of meters from the rupture show that these lateral variations in displacement are real and significant.

Rockwell and Klinger (2013) also note that the azimuth along which displacement is measured can have a significant effect on the estimation of displacement. They measured over 650 displacements along 15 km of the 1940 Imperial rupture at both the local fault strike and the average regional strike, and found that local differences can be as much as 25 % of the displacement value, whereas the end average using either azimuth is the same as long as one is consistent.

These new studies on lateral variability in displacement, along with how they are measured, have a direct impact on the results of our study from several perspectives. First, if an observer locks into an offset magnitude because of a high confidence measurement at one or more points along a stretch of rupture, there may be a tendency to try and repeat this offset value, even though the actual displacement has increased or dropped. Second, the magnitude of offset can be biased by the local fault strike if measurements are always taken along strike. Both of these factors can have a significant influence on the perception of overall displacement, the measurement of maximum displacement and other factors that are important in hazard analysis.

Conclusion

This work makes evident key challenges faced when remotely measuring fault-offset geomorphic features. The ability to which investigators can perform these tasks (making measurements, assigning uncertainties and quality ratings) is highly dependent on the geomorphic quality (i.e., preservation) of offset features and the digital representation of the features themselves. Fluvial channels in tectonically active regions constantly change, as degradation can begin immediately after formation in some cases. The longer-lived and larger the offset feature, the greater the uncertainty becomes, making slip estimates far into the past more difficult to interpret.

The UCERF3 database and our measurement validation survey provide a rich suite of data to build our understanding of the repeatability, accuracy, and precision of offset measurements. For all experience levels, major measurement discrepancies are typically gross errors that involve misinterpretation of the overall geologic features. The bulk of our results, however, suggest that the measurement methods in general are sound. Bond et al. (2007) showed that the more tools used in an interpretation, the better and more consistent the interpretation. We agree with that sentiment, considering field-validation can be a method of interpretation. However, we argue that while field validation can be useful for familiarization of fault zone characteristics, geographic region, etc., in many cases it can be unfeasible because of temporal,

financial, and land access limitations. For these reasons, the potential for LiDAR-based studies of active fault zones is pervasive and is something we must explore with a range of available tools. Standardizing measurement and reporting methods will be the crucial first step towards enhancing consistency of LiDAR-based analyses of active faults and establishing community protocols for future work.

Tables

Fault Name	Slope	R^2
Eureka Peak	0.08	-0.06
Johnson Valley	0.09	0.17
SAF	0.18	0.42
Homestead Valley	0.18	0.3
Elsinore	0.22	0.52
Emerson	0.22	0.28
Lavic Lake	0.23	0.45
Pisgah-Bullion	0.24	0.54
SJF	0.26	0.65
Panamint	0.26	0.62
Garlock	0.27	0.11
Owens Valley	0.32	-0.93
Mesquite Lake	0.35	0.56
Puente Hills	0.36	0.36
Calico-Hidalgo	0.52	0.87
Compton	0.61	0.27
Camp Rock	0.87	-0.04

Table 1. Trendline slopes and R^2 values of the line fit for uncertainty versus horizontal offset for the 17 fault strands shown in Figure 6 (those with >10 measurements with uncertainty estimates). Red highlights indicate historic earthquake ruptures that tend to be relatively more certain than the paleoseismic measurements.

Figures

Figure 1. Offset stream channel along the central Jacinto Fault near Anza, CA. Typical measurements of offsets are in the field. The two sets of people mark the location of the channel thalweg (bounded by the channel margins marked in green). These landform elements are project to the fault trace (marked in red) and the offset is the distance (horizontally or vertically) along the fault trace between the projected up and downstream elements.

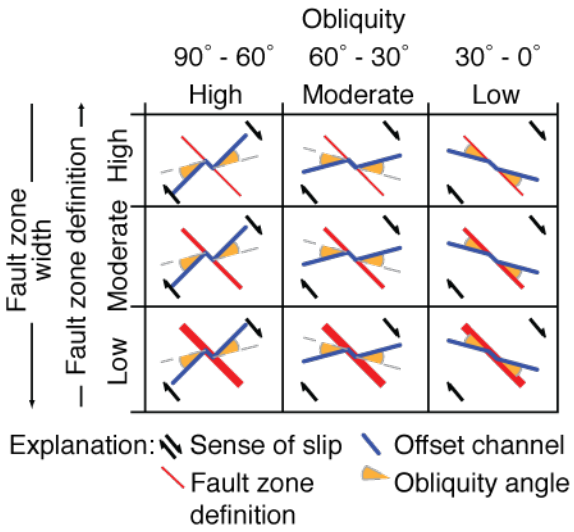

Figure 2. Channel obliquity and fault zone localization are two controls on the offset measurement quality. This basic quality rating rubric was developed by David Haddad and provided to validation experiment participants. The participants rated the quality first on the relative scale of obliquity and then fault zone width (e.g., for a channel at 25 degrees to a narrow, well defined fault trace "low-high").

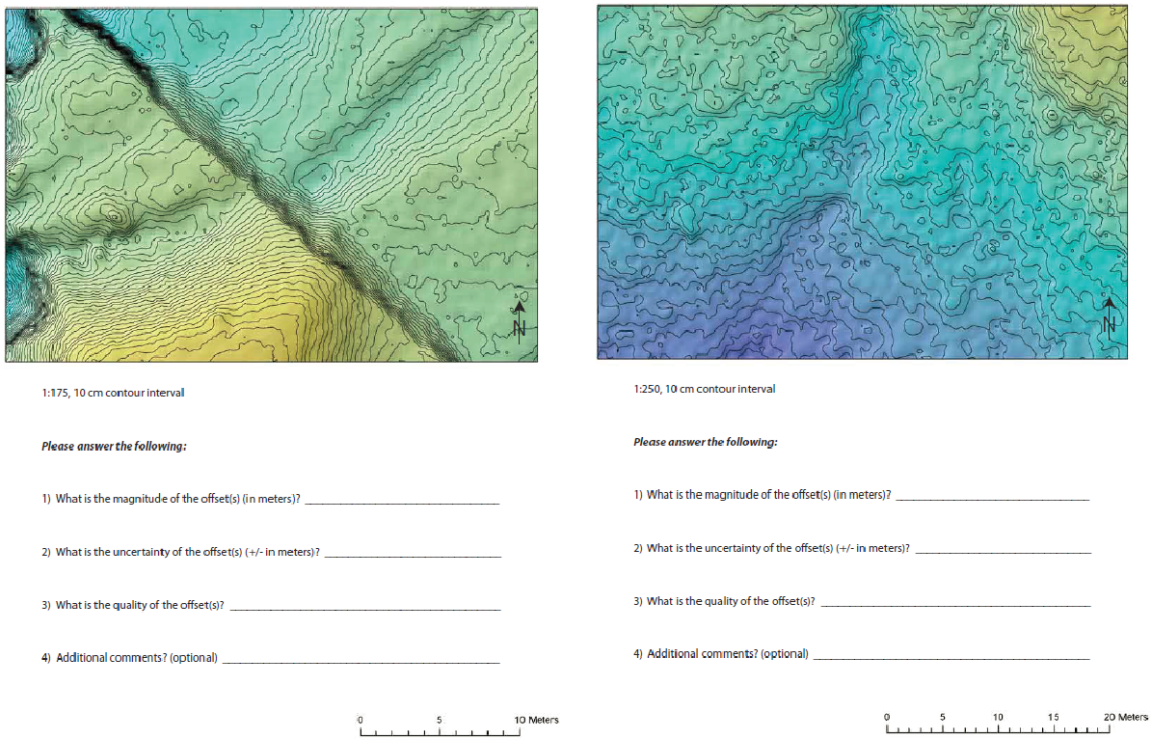

Figure 3. Two examples (of ten) offset channels and survey questions in the paper-based survey. The participant was asked to annotate the image with the fault trace, landform elements for reconstruction, and the offset and to measure the offset and uncertainty and rate the offset quality (see figure 3). The map scale and contour interval are indicated and were different for each example. Map scales ranged from 1:175 to 1:800 and the contour intervals were 10 cm to 100 cm.

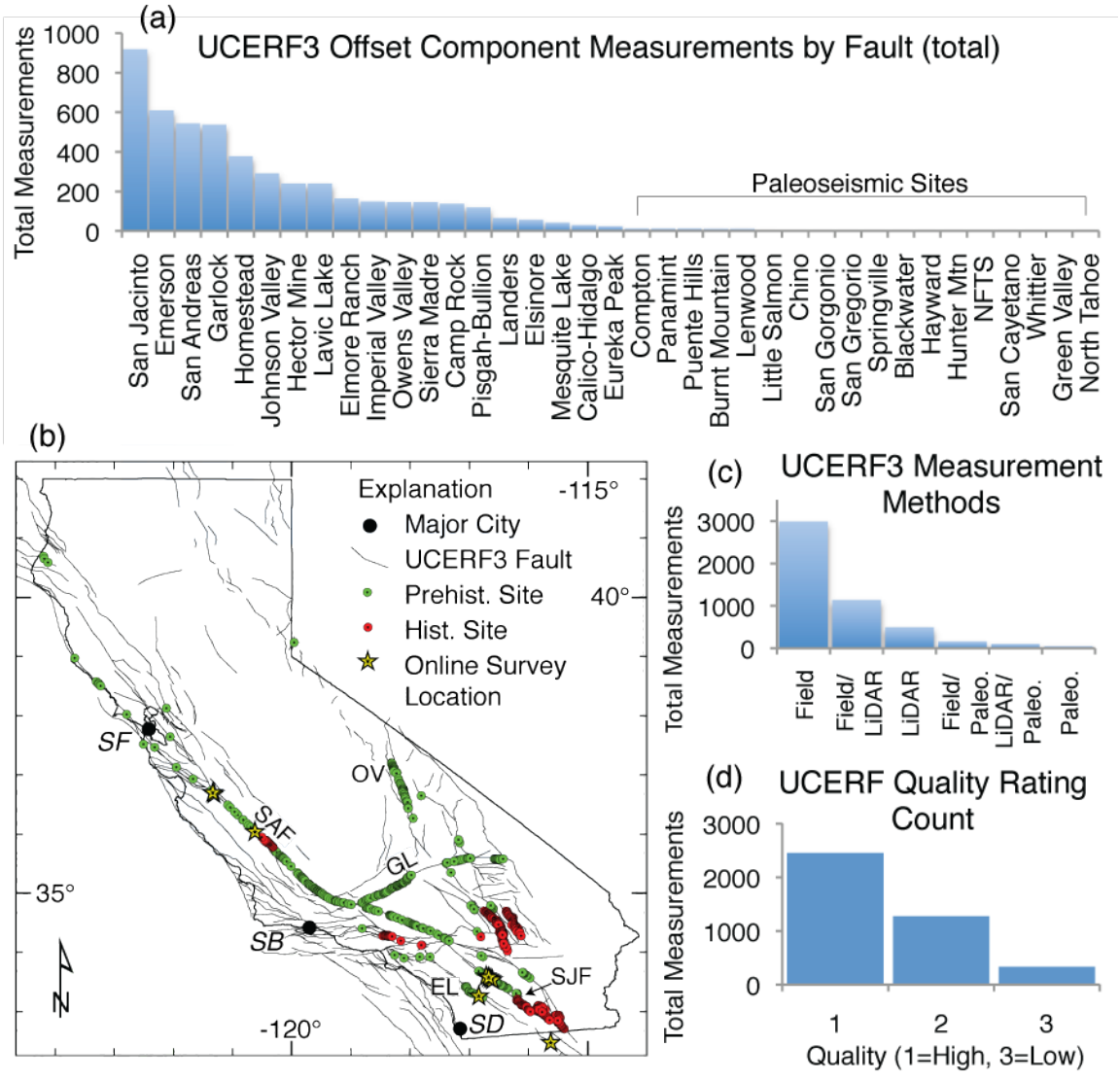

Figure 4 - Summary of historic and prehistoric EQ offset measurement components (horizontal and vertical displacement vectors) compiled for the UCERF3 database (Madden, et al., 2012). (a) Measurement tallies for fault strands, including paleoseismic sites. (b) Location map showing locations of historic (red) vs. prehistoric (green) measurement sites and geomorphic features selected for the online validation survey (yellow stars). Map of CA includes all fault segments defined by UCERF3. City name abbreviations: SF - San Francisco, SB – Santa Barbara, SD – San Diego. Fault name abbreviations: SAF – San Andreas, GL – Garlock, OV – Owens Valley, SJF – San Jacinto, EL – Elsinore. (c) Measurement method and (d) quality rating tallies for entire UCERF3 database, where 1 = high quality and 3 = low quality. Note that all existing displacement measurements without an associated quality rating were assigned a quality of "1" for the UCERF3 compilation and are mostly from the historic observations of surface rupture for which quality is usually high.

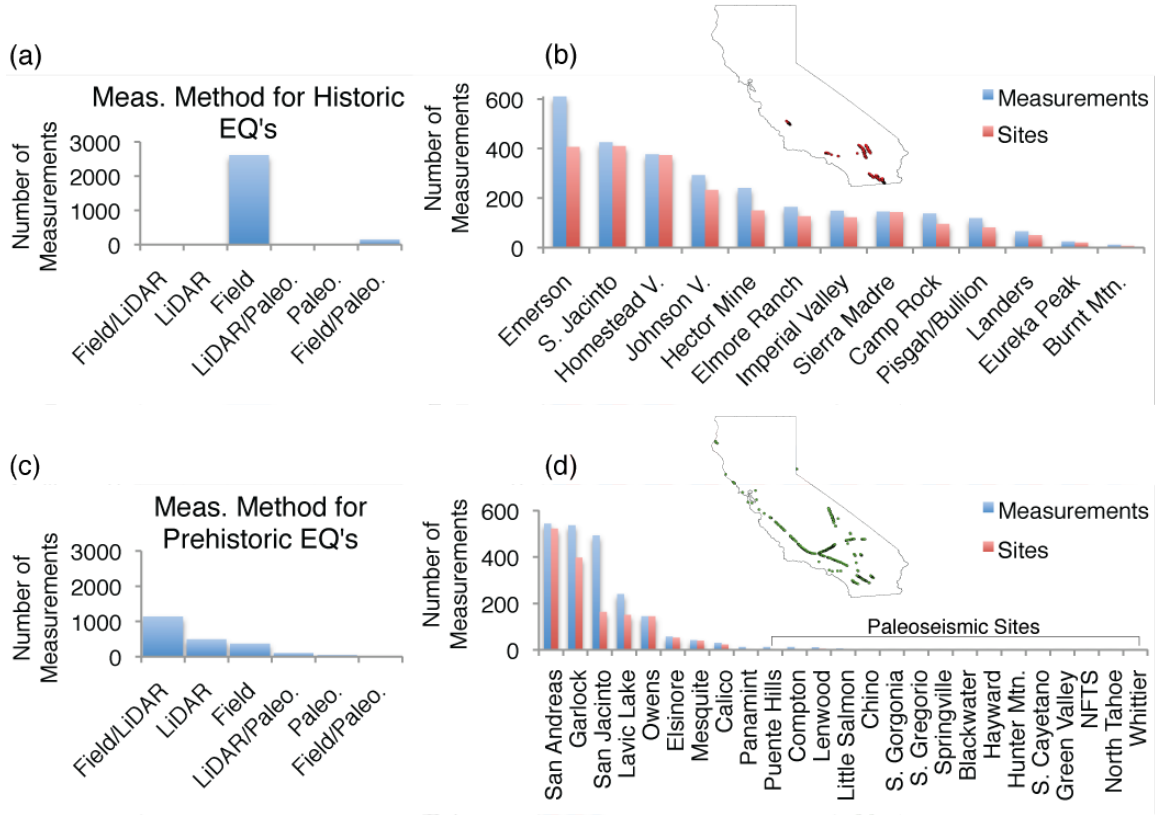

Figure 5 – Summary of UCERF3 database by classified event age: historic vs. prehistoric (Madden, et al., 2012). (a) Measurement method tally and (b) number of offset measurement components (blue) and unique geographic measurement sites (red) for historic EQ ruptures. Inset maps of CA show measurement locations. (c) Measurement methods tally and (d) number of offset measurement components (blue) and unique geographic measurement sites (red) for prehistoric EQ ruptures, including paleoseismic sites.

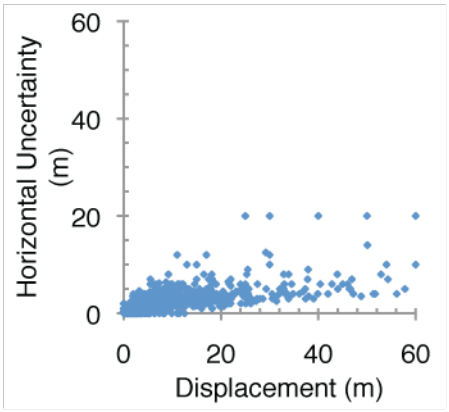

Figure 6. – Horizontal uncertainty versus displacement magnitude for the Calico-Hidalgo (30), Camp Rock (138), Compton (12), Elsinore (57), Eureka Peak (24), Emerson (610), San Andreas (544), San Jacinto (918), Garlock (537), Homestead Valley (377), Johnson Valley (292), Lavic Lake (240), Owens Valley (145), Panamint Valley (12), Pisgah-Bullion (119), and Puente Hills (12) faults, where the number in parentheses represents the total number of offset measurement components (Madden, et al, 2012).

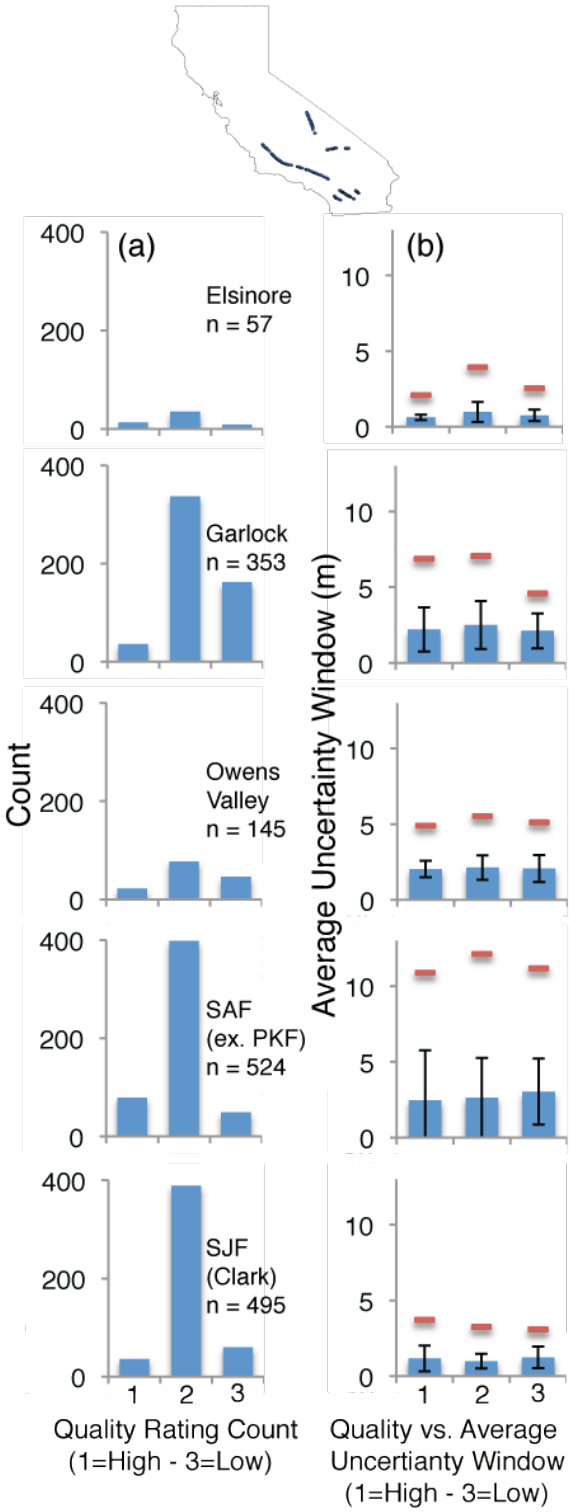

Figure 7 - Offset measurements generated for the UCERF3 data compilation (Elsinore, Garlock, Owens Valley, creeping San Andreas) or in the same analytical style (Cholame, Carrizo, Big Bend, Mojave, and Coachella portions of the SAF and the Clark strand of the SJF) where n represents the total number of component measurements (Madden, et al., 2012). Inset map of CA shows locations of measurements included in this analysis. Note that the Clark strand of the San Jacinto fault and the Coachella portion of the SAF include field-based measurements in addition to the LiDAR-derived measurements. The historic 2004 Parkfield EQ rupture measurements are not included in this particular analysis. (a) Quality rating count for new measurements, adapted from the original source to the UCERF3 quality-rating scheme. (b) Blue bars represent the average size of the uncertainty windows (difference between the maximum and minimum acceptable offsets for a given geomorphic feature) associated with measurements of a particular UCERF3 quality rating for each fault. Standard deviations are shown. Horizontal red lines indicate average offset magnitude for each group of measurements.

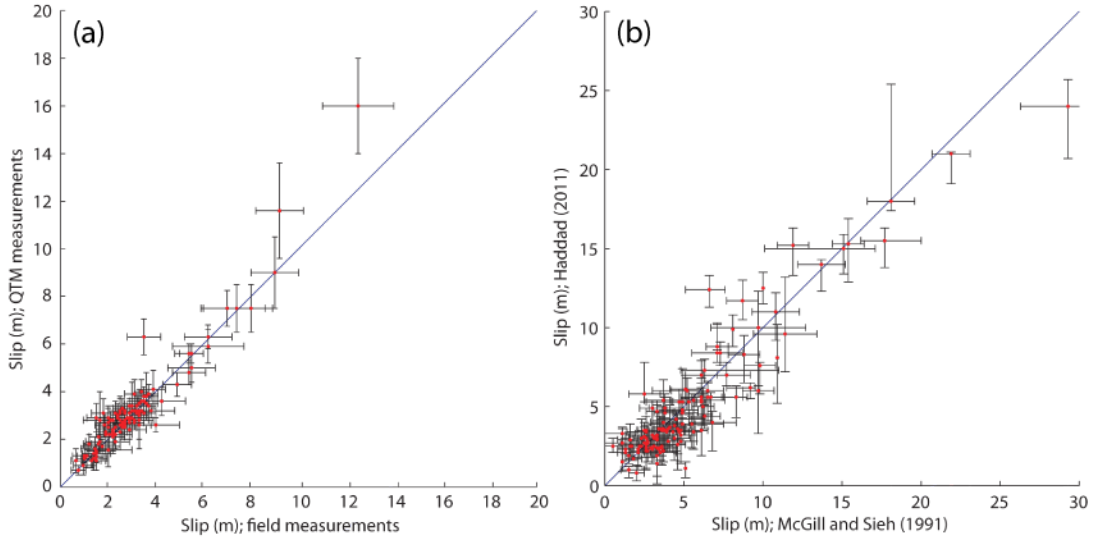

Figure 8. Field vs. LiDAR measurements a) made along the SJF by a single investigator (Salisbury et al., 2012) and b) along the GF, where LiDAR measurements are from Haddad (2011) and field measurements are from McGill and Sieh (1991).

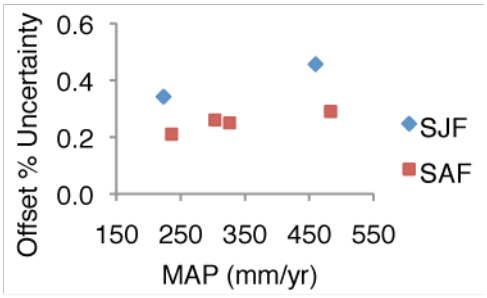

Figure 9 – Comparison of the average percent uncertainty associated with measurements made along portions of fault systems with differing mean annual precipitation (MAP) values. In both cases, a single investigator made measurements for each of the fault systems. Climate data provided by: PRISM Climate Group, Oregon State University, http://prism.oregonstate.edu, created 4 Feb 2004. MAP values were extracted and averaged along strike for portions of fault systems. The "SJF" points refer to the Clark strand, divided into two segments – to the northwest and southeast of Burnt Valley, and the "SAF" refers to the Cholame, Carrizo, Big Bend, and Mojave segments.

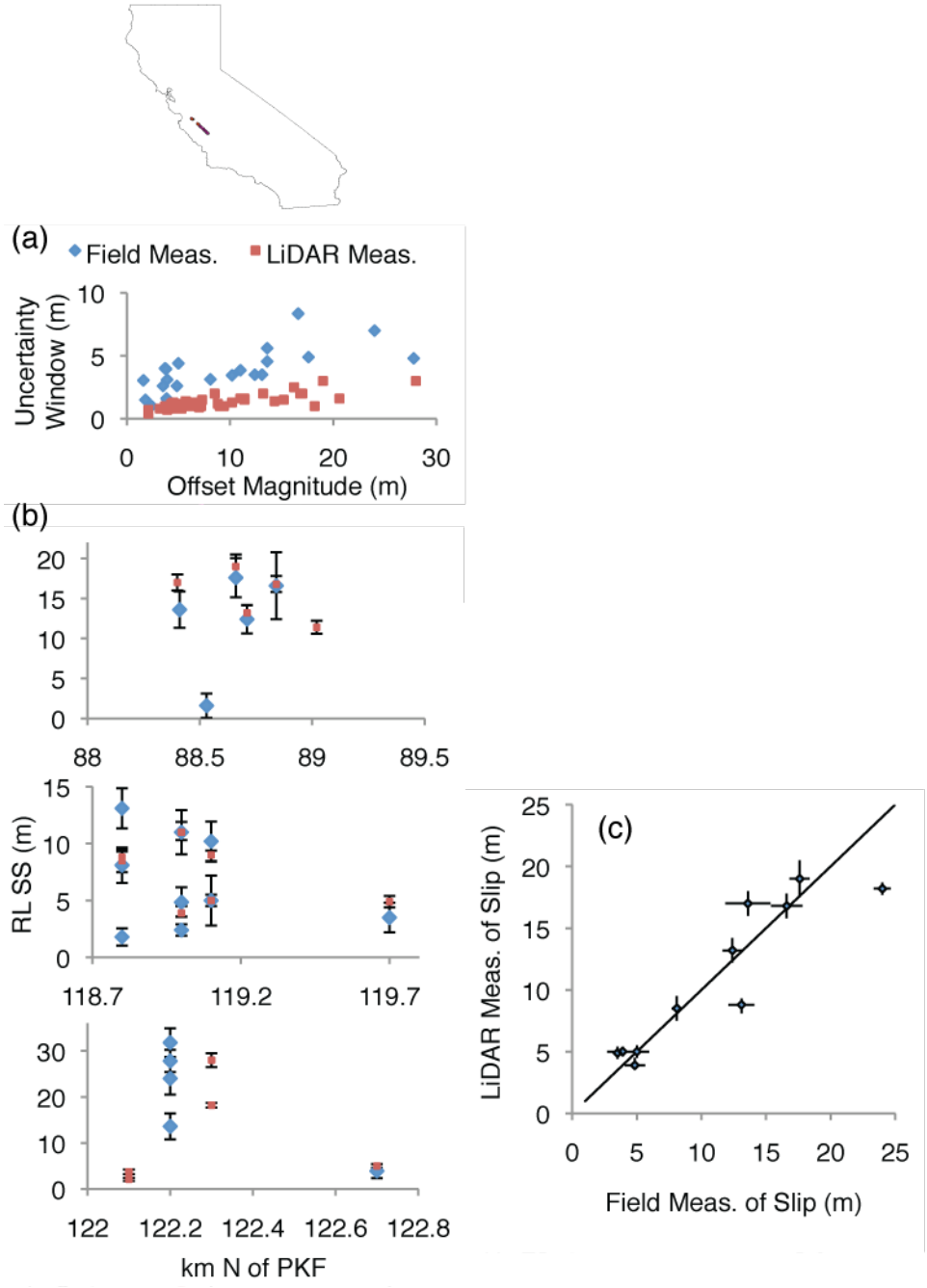

Figure 10 - Comparison of field- and LiDAR-based measurements (shown as blue diamonds and red squares, respectively) made along the creeping SAF between Parkfield and San Juan Bautista, CA for this study by Salisbury. Inset map of CA shows measurement locations. (a) Uncertainty windows versus offset magnitudes, and (b) displacement measurements with associated uncertainties along strike. (c) One-to-one comparison of field vs. LiDAR measurements where both exist for the same geomorphic feature.

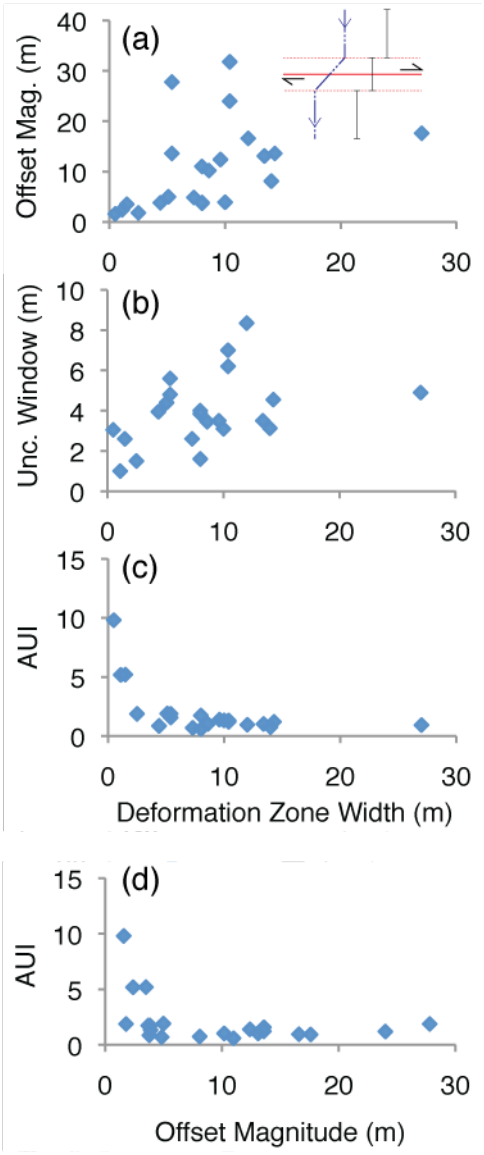

Figure 11 - Summary of field-based offset measurement metrics for the creeping SAF. For each feature visited in the field, we measure the length of the upstream and downstream channel segments, as well as the width of the perceived deformation zone. See inset figure for diagram. Channel segments were made within the thalweg and the deformation zone width was measured normal to the fault trace. We calculate the Average Uncertainty Index (AUI) as an average of the ratios between the channel segment length and deformation zone width for both the upstream and downstream channel segments. (a) Offset magnitude in meters versus deformation zone width, (b) uncertainty window versus deformation zone width, (c) AUI versus deformation zone width, and (d) AUI versus total offset magnitude.

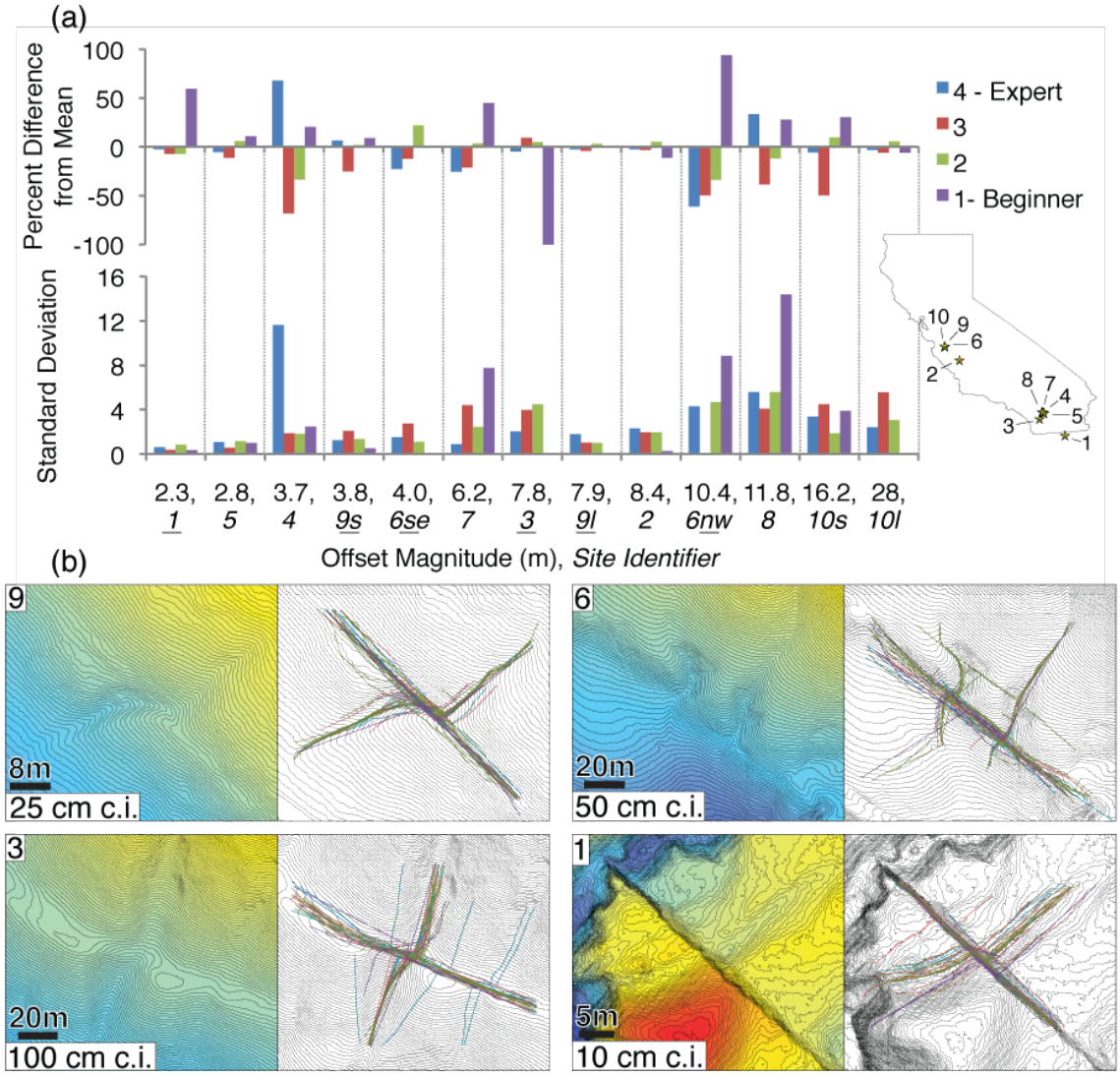

Figure 12 – Results of the Google Earth portion of the online offset validation experiment: 28 Google Earth "path" files in *.kmz format. Locations of the 10 features chosen for the experiments are shown on the inset map. (a) The 10 features are arranged in order of the average offset magnitude estimate. This average is also used for percent difference from mean and standard deviation calculations for each experience level (color coded). Site identifiers are shown in italics, where the "s" and "l" stand for "small" and "large" offsets recorded in the same features, and the "se" and "nw" stand for "southeast" and "northwest" channels within the same frame. Sites shown in part (b) are underlined. (b) Four of the offset features chosen for the study with the site identifier located in the upper left corner. The first color image shows the geomorphic features (dry channels, in all of these cases) with scale bar and labeled contour interval (c.i.). Warmer colors represent higher elevations. The second image shows the submitted interpretations color-coded according to experience level (colors as in Figure 11a)

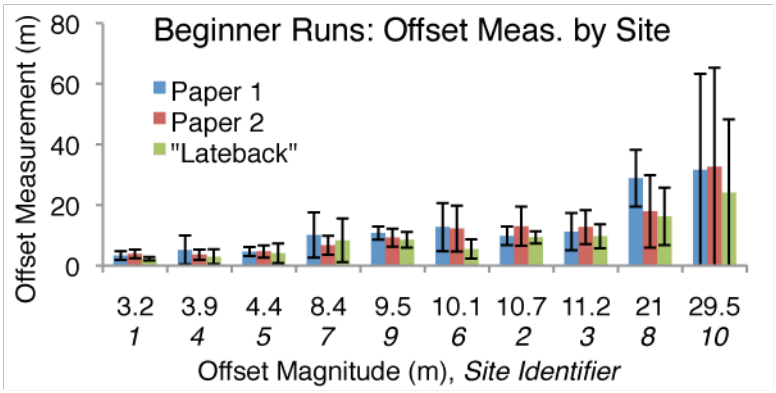

Figure 13 – Results of the "classroom" validation experiments (i.e. all participants are experience level 1 or 2). Features are again organized according to the average estimate of displacement with site identifiers listed in italics below offset magnitude. "Paper 1" refers to a group of undergraduate and graduate students in an upper-level geomorphology class prior to an introductory lecture on strike-slip faulting, whereas "Paper 2" refers to the same group of students a week after the lecture on strike-slip faulting. "Lateback" refers to a second group of undergraduate students using a Matlab-based GUI to estimate the amount of backslip necessary to reconstruct tectonic offset. Average offset measurements and standard deviations shown for each feature by each group.

References

The Working Group on California Earthquake Probabilities (WGCEP), *Probabilities of large earthquakes occurring in California along the San Andreas fault; USGS Open File Report 88-398*, 1988

Akciz, S. O., L. Grant-Ludwig, J. R. Arrowsmith, and O. Zielke (2010). Century-long average time intervals between ruptures on the San Andreas Fault in the Carrizo Plain, *Geology.*

Audemard, F. A., R. Ollarves. M. Bechthold, G. Diaz, C. Beck, E. Carrillo, D. Pantosti, and H. Diederix (2008). Trench investigation on the main strand of the Bocono fault in its central section, at Mesa del Caballo, Merida Andes, Venezuela, *Tectonophysics, 459*, 38-53.

Awata, Y., B. Fu, and Z. Zhang (2010). Geometry and slip distribution of the 1931 Fuyun Surface Rupture, northwest China. Forecasting large earthquakes from active faults in time and space, HOKUDAN International Symposium on active faulting.

Bond, C. E., Gibbs, A. D., Shipton, Z. K., and S. Jones (2007). What do you think this is? "Conceptual uncertainty" in geoscience interpretation, *GSA Today*, v. 17, no. 11, doi: 10.1130/GSAT01711A.1

Bond, C. E., Philo, C., and Z. K. Shipton (2011). When There isn't a Right Answer: Interpretation and reasoning, key skills for twenty-first century geoscience, *Int. Journal of Sci. Education*, v. 33, no. 5, pp. 629-652.

Burbank, D. W. and R. S. Anderson (2001). Tectonic geomorphology, 1st ed., Blackwell Science Inc., Malden, MA.

Cowgill, E., (2007). Impact of riser reconstruction on estimation of secular variation in rates of strike-slip faulting: Revisiting the Cherchen River site along the Altyn Tagh fault, NW China, *Earth Planet. Sci. Lett., 254*, 239-255.

Grant-Ludwig, L., S. O. Akciz, G. R. Noriega, O. Zielke, and J. R. Arrowsmith (2010). Climate-modulated channel incision and rupture history of the San Andreas Fault in the Carrizo Plain, *Science*, *327*, no. 5969, 1117-1119.

Hauessler, P. J., D. P. Schwartz, T. E. Dawson, H. D. Stenner, J. J. Lienkaemper, B. Sherrod, F. R. Cinti, P. Montone, P. A. Craw, A. J. Crone, and S. F Personius (2004). Surface rupture and slip distribution of the Denali and Totschunda faults in the 3 November 2002 M7.9 earthquake, Alaska, *Bull. Seis. Soc. Am., 94(6B)*, S23-S52.

Klinger, Y., M. Etchebes, P. Tapponnier, and C. Narteau (2011), Characteristic slip for five great earthquakes along the Fuyun fault in China, Nature Geosci. 4, 389-392, DOI: 10.1038/NGEO1158.

Kondo, H., Y. Awata, Ö. Emre, A. Doğan, S. Özalp, F. Tokay, C. Yildirim, T. Yoshioka, and K. Okumura (2005). Slip distribution, fault geometry, and fault segmentation of the 1944 Bolu-Gerede earthquake rupture, North Anatolian fault, Turkey, *Bull. Seis. Soc. Am.*, 95, 1234-1249.

Kondo, H. V. Özaksoy, and C. Yildirim (2010). Slip history of the 1944 Bolu-Gerede earthquake rupture along the North Anatolian fault system – Implications for recurrence behavior of multi-segment earthquakes, *in press*, *J. Geophys. Res.,* 2009JB006413.

Leprince, S., K.W. Hudnut, S. Akciz, A. Hinojosa Corona, and J.M. Fletcher, "Surface rupture and slip variation induced by the 2010 El Mayor – Cucapah earthquake, Baja California, quantified using COSI-Corr analysis on pre- and post-earthquake LiDAR acquisitions." (2011 SCEC Annual Meeting poster).

Lienkaemper, J. J. (2001). 1857 Slip on the San Andreas Fault Southeast of Cholame, California, *Bull. Seis. Soc. Am.*, *91(6)*, 1659-1672.

Madden, C., D. E. Haddad, J. B. Salisbury, O. Zielke, J. R. Arrowsmith, J. Colunga, and R. J. Weldon II (2012). Uniform California Earthquake Rupture Forecast, Version 3 (UCERF3) Framework, Working Group on California Earthquake Probabilities (WGCEP), Technical Report #8; Appendix R: Compilation of Slip in the Last Event Data and Analysis of Last Event, Repeated Slip, and Average Displacement for Recent and Prehistoric Ruptures.

McCalpin, J. (2009). Paleoseismology, 2nd ed., Academic Press, San Diego, CA.

McGill, S. F., and K. E. Sieh (1991). Surficial offsets on the central and eastern Garlock fault associated with prehistoric earthquakes, *J. Geophys. Res. 96 (B13)*, 21597-21621.

Nissen, E., Krishnan*, A. K., Arrowsmith, J R., Saripalli, S., Three-dimensional surface displacements and rotations from differencing pre- and post-earthquake Lidar point clouds, Geophysical Research Letters, v. 39, L16301, doi:10.1029/2012GL052460, 2012.

Oskin, M., Arrowsmith, J.R., Corona, A.H., Elliott, A.J., Fletcher, J.M., Fielding, E., Gold, P.O., Garcia, J.J.G., Hudnut, K.W., Liu-Zeng, J., Teran, O. J. (2012). Complex surface rupture of the El Mayor-Cucapah earthquake imaged with airborne lidar: Science, v. 335, p. 702-705.

Ouchi, S. (2004). Flume experiments on the horizontal stream offset by strike-slip faults, *Earth Surf. Process. Landforms, 29,* 161-173, DOI: 10.1002/esp.1017.

Rockwell, T. K. (1990). Holocene activity of the Elsinore fault in the Coyote Mountains, Southern California, in *Friends of the Pleistocene Winter Fieldtrip: Western Salton Trough Soils and Neotectonics*, San Diego State University, San Diego, California, 30-42.

Rockwell, T. K. and C. T. Pinault (1986). Holocene slip events on the southern Elsinore fault, Coyote Mountains, southern California, in *Neotectonics and Faulting in Southern California*, P. Ehlig (Editor), Geol. Soc. Am. Guidebook and Volume, Cordilleran Section, Boulder, Colorado, 193-196.

Rockwell, T.K. and Y. Klinger, (2013) Surface Rupture and Slip Distribution of the 1940 Imperial Valley Earthquake, Imperial Fault, Southern California: Implications for Rupture Segmentation and Dynamics, Bulletin of the Seismological Society of America, in press for March issue.

Salisbury, J. B., T. K. Rockwell, T. Middleton, and K. Hudnut (2012). LiDAR and field observations of slip distribution for the most recent surface ruptures along the central San Jacinto fault, *Bull. Seis. Soc. Am., 102(2)*, 598-619.

Scharer, K., Salisbury, J. B., Arrowsmith, J R., 2012 SoSAFE Fieldshop Report, 2012.

Scholz, C. H. (2002). The Mechanics of Earthquakes and Faulting, 2nd ed., Cambridge Univ. Press, Cambridge, U.K.

Schwartz, D. P. and K. J. Coppersmith (1984). Fault behavior and characteristic earthquakes: examples from the Wasatch and San Andreas fault zones, *J. Geophys. Res.,* 89(B7), 5681-5698.

Sieh, K. E. (1978). Slip along the San Andreas fault associated with the great 1857 earthquake, *Bull. Seis. Soc. Am., 68(5)*, 1421-1448.

Sieh, K. E. and R. H. Jahns (1984). Holocene activity of the San Andreas fault at Wallace Creek, California, *Geol. Soc. Am. Bull.*, 95, 883-896.

Shimazaki, K. and T. Nakata (1980). Time-predictable recurrence model for large earthquakes, *Geophys. Res. Lett.*, 7(4), 279-282.

Trifonov, V. G., V. I. Makarov, and S. F. Skobelev (1992). The Talas-Fergana active right-lateral fault, *Ann. Tectonicae*, v.5, suppl. 224-237.

Wallace, R. E. (1968). Notes on stream channels offset by the San Andreas fault, southern coast ranges, California, in *Prof. of Conf. on Geological Problems of the San Andreas Fault system,* W. R. Dickson and A. Grantz, Eds., *Stanford Univ. Publ., Geol. Sci., Univ. Ser., 11,* 6-21.

Wallace, R. E., ed. (1990). The San Andreas fault system, California, *U.S. Geol. Surv. Prof. Pap., 1515*, 3-21.

Washburn, Z., J. R. Arrowsmith, S. L. Forman, E. Cowgill, X. F. Wang, Y. Q. Zhang, and Z. L. Chen (2001). Late Holocene earthquake history of the central Altyn Tagh fault, China, *Geology*, 29(Nov), 1051-1054.

Yeats, R. S., K. E. Sieh, and C. R. Allen (1997). The Geology of Earthquakes, Oxford University Press, Oxford, New York, 568 pp.

Zielke, O., J. R. Arrowsmith, L Grant Ludwig, and S. O. Akciz (2010). Slip in the 1857 and earlier large earthquakes along the Carrizo Plain, San Andreas Fault, *Science, 327*, 1119-1122.

Zielke, O., and J R. Arrowsmith (2012). LaDiCaoz and LiDARimager -MATLAB GUIs for LiDAR data handling and lateral displacement measurement, *GeoSphere Special issue on high resolution topography*, v. 8, no. 1, p. 206–221, doi:10.1130/GES00686.1.

Zielke, O., Arrowsmith, J R., Grant Ludwig, L., Akciz, S. O. (2012). High resolution topography-derived offsets along the 1857 Fort Tejon earthquake rupture trace, San Andreas Fault, *Bulletin of the Seismological Society of America*, doi: 10.1785/0120110230, vol. 102 no. 3 1135-1154.